Article

Chemical Imaging of Corrosion: Sum Frequency Generation Imaging Microscopy of Cyanide on Gold at the Solid#Liquid Interface

Katherine Cimatu, and Steven Baldelli

J. Am. Chem. Soc., **2008**, 130 (25), 8030-8037 • DOI: 10.1021/ja8011676 • Publication Date (Web): 03 June 2008

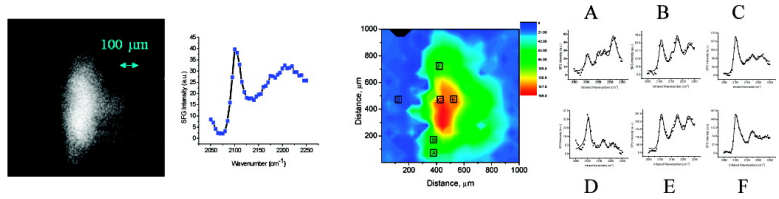

More About This Article

Additional resources and features associated with this article are available within the HTML version:

- Supporting Information
- Links to the 2 articles that cite this article, as of the time of this article download
- Access to high resolution figures
- Links to articles and content related to this article
- Copyright permission to reproduce figures and/or text from this article

View the Full Text HTML

Journal of the American Chemical Society is published by the American Chemical Society. 1155 Sixteenth Street N.W., Washington, DC 20036

J|A|C|S
ARTICLES

Published on Web 06/03/2008

Chemical Imaging of Corrosion: Sum Frequency Generation Imaging Microscopy of Cyanide on Gold at the Solid−Liquid Interface

Katherine Cimatu and Steven Baldelli*

Department of Chemistry, University of Houston, Houston, Texas 77204-5003

Received February 15, 2008; E-mail: SBaldelli@uh.edu

Abstract: Sum frequency generation (SFG) imaging is used to monitor, in situ, the reaction of cyanide ions with gold surface. Spatial and chemical variations across the surface are observed as a function of time. The initial period resulted in the formation of linearly bound cyanide to gold, and continuous exposure of gold film to cyanide solution led to the presence of higher-coordinated gold−cyanide complexes. These species were identified by their specific position in the SFG vibrational spectrum (2105, 2140, 2170, and 2225 cm^{-1}). The relative amounts of these gold−cyanide species varied across the surface as resolved by SFG microscopy.

Introduction

The corrosion of metals and methods to inhibit it are two of the most important problems confronted in industry.[1] Exposure of metal surfaces to moisture or active reagent causes the metal to react and form oxidation products.[2] The process of etching is a form of corrosion; for example, the etching of gold. In the presence of CN^-, gold can be oxidized by O_2 to form Au(I) and Au(III) complexes.[3] This reaction is known to form different complex products as CN^- attacks the Au atom and removes it from the surface into solution.[3]

Most metals, such as gold, silver, copper, and mild steel, have been studied for occurrences of corrosion using spectroscopy and microscopy, independently.[4,5] Different techniques have been used to characterize and observe in situ and ex situ reactions of cyanide with metal surfaces. The reaction depends on several factors: the exposure time, concentration of cyanide species, presence of dissolved oxygen, quality of the metal substrate, and/or its dependence toward change in applied potential. Several techniques were used to specifically characterize the surfaces of metals with cyanide as the etchant. Infrared (IR) spectrocopy[6–8] and surface-enhanced Raman scattering/spectroscopy (SERS)[5,9–13] helped determine and identify the vibrational peaks after exposing the gold metal to cyanide ions. Table 1 presents the vibrational peak assignments for the linearly adsorbed CN^- on gold and gold−cyanide complexes involved in the reaction of cyanide with the gold metal. The peak at 2105 cm^{-1} is assigned to be the linearly adsorbed CN^- on Au.[7,12] Detailed infrared and Raman spectroscopy studies on Au−CN complexes in solution and solid state have been performed by Jones et al. These investigations assigned the peaks at 2140, 2170, and 2190−2230 cm^{-1} to $[Au(CN)_2]^-$ (symmetric and asymmetric stretches) and $[Au(CN)_4]^-$ stretch, respectively.[7,12,14–17] In addition, the possibility of oxidized products such as Au−OCN and complexes $H[Au(CN)_4]$ was proposed for peaks above 2200 cm^{-1}.[16–18] The observed sum frequency generation (SFG) peaks are within a range of ± 10 cm^{-1} from those quoted in the references.[6]

Table 1. Peak Assignments of the C≡N Vibrational Modes within the 2050−2250 cm^{-1} Region[7,12,14–17,20] [a]

peak assignment (cm^{-1})	vibrational modes
2105	linear CN^- on-top geometry (CN adsorbed on Au)[7]
2140	$[Au(CN)_2]^-$ dicyanoaurate(I) ion symmetric stretch[6]
2170	$[Au(CN)_2]^-$ dicyanoaurate(I) ion asymmetric stretch[6]
2190−2225	$[Au(CN)_4]^-$ C≡N stretch[7] tetracyanoaurate(III) ion, above 2200 cm^{-1} Au−OCN or $H[Au(CN)_4]$ solid[18,19]

[a] The peaks at ∼2170 and 2225 cm^{-1} seem to be due to the Au(III) complex based on their spatial and time dependents in the SFG measurement.

Several in situ spectroscopy and electrochemical investigations have been performed. The application of external potential

(1) Jones, D. A. *Principles and Prevention of Corrosion*, 2nd ed.; Prentice Hall: Upper Saddle River, NJ, 1996.
(2) Leygraf, C.; Graedel, T. *Atmospheric Corrosion*, 1st ed.; Wiley & Sons: New York, 2000.
(3) Watling, K.; Hope, G. A.; Woods, R. *J. Electrochem. Soc.* **2005**, *152*, D103.
(4) Cooper, D.; Plane, R. A. *Inorg. Chem.* **1966**, *5*, 16.
(5) Corrigan, D. S.; Gao, P.; Leung, L.-W. H.; Weaver, M. J. *Langmuir* **1986**, *2*, 744.
(6) Kunimatsu, K.; Seki, H.; Golden, W. G.; Gordon, J. G., II; Philpott, M. R. *Langmuir* **1988**, *4*, 337.
(7) Huerta, F.; Mele, C.; Bozzini, B.; Morallon, E. *J. Electroanal. Chem.* **2004**, *569*, 53.
(8) Kim, C. S.; Korzeniewski, C. *J. Phys. Chem.* **1993**, *97*, 9784.
(9) Baltruschat, H.; Heitbaum, J. *J. Electroanal. Chem.* **1983**, *157*, 319.
(10) Gao, P.; Weaver, M. J. *J. Phys. Chem.* **1989**, *93*, 6205.
(11) Gao, P.; Weaver, M. J. *J. Phys. Chem.* **1986**, *90*, 4057.
(12) Bozzini, B.; Fanigliulo, A. *J. Appl. Electrochem.* **2002**, *32*, 1043.
(13) Pettinger, B.; Picardi, G.; Schuster, R.; Ertl, G. *J. Electroanal. Chem.* **2003**, *554*−*555*, 293.
(14) Mazur, U.; Williams, S. D.; Hipps, K. W. *J. Phys. Chem.* **1981**, *85*, 2305.
(15) Jones, L. H. *Inorg. Chem.* **1964**, *3*, 1581.
(16) Jones, L. H. *J. Chem. Phys.* **1965**, *43*, 594.
(17) Smith, J. M.; Jones, L. H.; Kressin, I. K.; Penneman, R. A. *Inorg. Chem.* **1965**, *4*, 369.
(18) Jones, L. H.; Smith, J. M. *J. Chem. Phys.* **1964**, *41*, 2507.
(19) McCarley, R. L.; Bard, A. J. *J. Phys. Chem.* **1992**, *96*, 7410.

10.1021/ja8011676 CCC: $40.75

greatly affected the vibrational frequencies of the linear adsorbed CN^- by the Stark effect.[9] In one study, Gao and Weaver used mixed isotopes of $^{12}CN^-/^{13}CN^-$ as samples and SERS and IR techniques to reveal that there is a weak vibrational coupling between the linearly adsorbed cyanide species.[10] Philpott's group observed the existence of the Au dicyanide complex, $[Au(CN)_2]^-$, with two distinct vibrational modes that differ by approximately 10 cm^{-1} and were assigned to be the symmetric and asymmetric vibrational stretches.[6] Watling et al. investigated the dissolution of gold in Cl^- and CN^- solution by SERS. They observed the formation of linear Au−CN and $[Au(CN)_2]^-$ as well as the possibility of Au−OCN oxidation product.[3] These results provided vibrational spectroscopic identification of the gold−cyanide species as reaction products bound to the surface.

Nonspectroscopic techniques, with high spatial resolution, had also been used to study cyanide reactions with gold. McCarley and Bard[19] performed the first in situ scanning tunneling microscopy (STM) and observed monolayer pit formation using aqueous cyanide solution as the chemical etchant. Ex situ and in situ analyses were used to compare the results after exposure of the gold metal surface in dilute cyanide solution.[13,14,19] Several groups have also studied this phenomenon using Au(111) in acidic and alkaline KCN with in situ STM.[21] This technique provided images on the formation of pits and displacement of gold atoms (atomic scale) upon exposure of gold surface to cyanide solution.

Previously, SFG spectroscopy was also used to provide information on the formation of gold cyanide surface species. Several groups specializing in SFG spectroscopy have already studied cyanide adsorption on different metal surfaces such as platinum, copper, silver, and gold.[22–27] The in situ SFG results on platinum surfaces exposed on cyanide solutions observed two vibrational modes that were assigned to be the linearly bound cyanide on the Pt surface and the other peak to be a high-frequency band arising from a microscopic surface disorder or CN^- bound to surface defects.[22] For CN^- on copper, platinum, silver, and gold metals, difference frequency generation and SFG spectroscopy were used to measure the lifetime of cyanide vibrational stretching mode after application of potential.[24,25] These SFG results provided significant vibrational assignments of cyanide on specific single crystalline surfaces. However, additional information is still needed about the cyanide−gold reaction at the interface, especially under more aggressive reaction conditions and the presence of spatially and chemically distinct surface species.

The $CN^-/Au/O_2$ system has been studied in some detail, although not all steps are known. Since the reaction is a surface occurrence, interface specific techniques are useful to the investigation of the etching process of gold and formation of local corrosion products. To obtain spectral and spatial information, the sum frequency generation imaging microscopy (SFGIM) is used; the SFGIM has an advantage of identifying the local corrosion products at different regions of interest (ROI) on the basis of their unique vibrational spectrum. As a result, SFGIM has detected the in situ formation and evolution of different cyanide species (formation of gold−cyanide complexes) spectroscopically and spatially at the solid−liquid interface. This article focuses on the etching of gold metal surface observed using SFGIM and the simultaneous formation and evolution of the surface species. These species present are the linearly attached CN^- on gold and gold−cyanide complexes that vary in concentration and location across the gold surface.

SFG Theory

Sum frequency generation is a second-order nonlinear process that is used to detect molecules at the interface.[28] The technique involves the overlap of two pulsed laser beams at the surface generating a third beam with a frequency that is the sum of the two input frequencies. This process is proportional with SFG intensity, I_{SF}, which is defined as follows:

$$I_{SF} \propto \left| \sum_{JK} \chi_{IJK}^{(2)} E_J(\omega_{vis}) E_K(\omega_{IR}) \right|^2 \quad (1)$$

where $\chi_{IJK}^{(2)}$ is the second-order nonlinear surface susceptibility and the $E(\omega)$ terms are light field amplitudes. The susceptibility tensor, $\chi_{IJK}^{(2)}$, contains the information on the properties of the interface. The resonant portion contains the vibrational information of the molecules, $\chi^{(2)}{}_R$, while the nonresonant susceptibility is primarily due to the gold substrate, $\chi^{(2)}{}_{NR}$:

$$\chi^{(2)} = \chi_R^{(2)} + \chi_{NR}^{(2)} = \sum_q \frac{A_q}{\omega_{IR} - \omega_q + i\Gamma} + \chi_{NR}^{(2)} \quad (2)$$

where ω_{IR} and ω_q are the infrared frequency and the resonant frequency of the qth vibrational mode, respectively. The damping factor of the vibration is Γ.

Because SFG is a $\chi^{(2)}$ process, a signal is only generated in a medium that lacks inversion symmetry, such as the surface. When the IR light comes into resonance with a surface vibrational mode, there is an increase in the nonlinear susceptibility, $\chi^{(2)}$. Therefore, a plot of infrared wavelength vs sum frequency intensity is interpreted as the vibrational spectrum of the molecules on the surface. Because of phase matching conditions, SFG output is coherent and directional, which allows for efficient collection of signal photons.[29–34]

Experimental Section

Materials. The gold shots with 99.99% purity were purchased from Americana Precious Metals. The chromium rods (99.9% purity) were obtained from R. D. Mathis Co. The single-crystal silicon (100) wafers were acquired from Silicon Sense, Inc. and had a polished and unpolished side. The wafers are cleaned with absolute ethanol (200 proof) purchased from AAPER Alcohol.

Preparation of Gold Thin Film. The Si wafers were attached to the rotating plate of the thermal evaporator after being rinsed with absolute ethanol and dried with a nitrogen gas. A thin film of

(20) Nakamoto, K. *Infrared and Raman Spectra of Inorganic and Coordination Compounds*, 3rd ed.; Wiley & Sons: New York, 1978.
(21) Shue, C. H.; Yau, S.-L.; Itaya, K. *J. Phys. Chem. B* **2004**, *108*, 17433.
(22) Friedrich, K.; Daum, W.; Klunker, C.; Knabben, D.; Stimming, U.; Ibach, H. *Surf. Sci.* **1995**, *335*, 315.
(23) Tadjeddine, M.; Flament, J.-P.; Le Rille, A.; Tadjeddine, A. *Surf. Sci.* **2006**, *600*, 2138.
(24) Matranga, C.; Wehrenberg, B. L.; Guyot-Sionnest, P. *J. Phys. Chem. B* **2002**, *106*, 8172.
(25) Matranga, C.; Guyot-Sionnest, P. *J. Chem. Phys.* **2000**, *112*, 7615.
(26) Tadjeddine, A.; Le Rille, A. *Electrochem. Acta* **1999**, *45*, 601.
(27) Dederichs, F.; Petukhova, A.; Daum, W. *J. Phys. Chem. B* **2001**, *105*, 5210.
(28) Bain, D. C. *J. Chem. Soc., Faraday Trans.* **1995**, *91*, 1281.
(29) Hunt, J. H.; Guyot-Sionnest, P.; Shen, Y. R. *Chem. Phys. Lett.* **1987**, *133*, 189.
(30) Superfine, R.; Huang, J. Y.; Shen, Y. R. *Chem. Phys. Lett.* **1990**, *172*, 303.
(31) Baldelli, S.; Mailhot, G.; Ross, P. N.; Shen, Y. R. *J. Phys. Chem. B* **2001**, *105*, 654.
(32) Baldelli, S. *J. Phys. Chem. B* **2003**, *107*, 6148.
(33) Baldelli, S.; Markovic, N.; Ross, P.; Shen, Y.-R.; Somorjai, G. *J. Phys. Chem. B* **1999**, *103*, 8920.
(34) Superfine, R.; Guyot-Sionnest, P.; Hunt, J. H.; Kao, C. T.; Shen, Y. R. *Surf. Sci.* **1988**, *200*, L445.

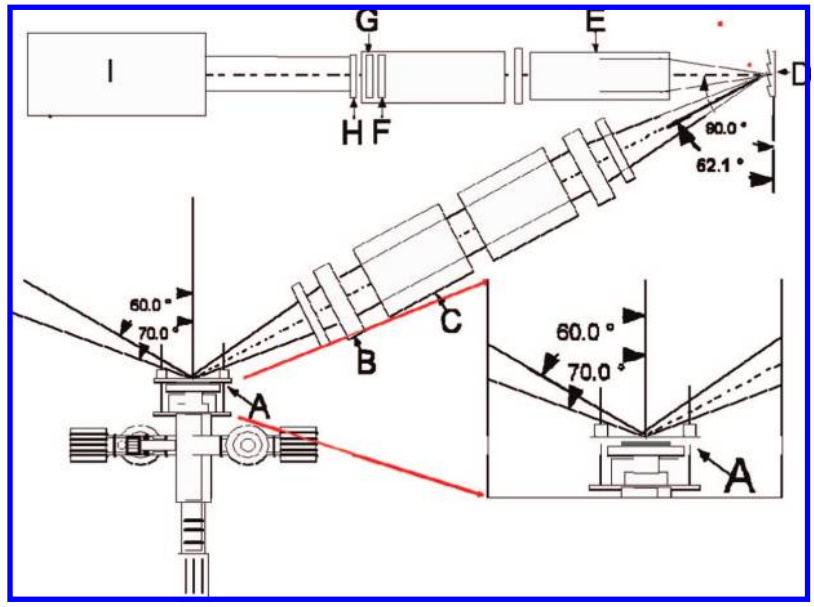

Figure 1. Schematic diagram of the SFGIM setup used in the Au−CN^- experiment. The beams overlap at the sample surface at specific angles. (A) An SFG cell was used where the gold slide was put in between CaF_2 window and the Teflon base. A thin layer of cyanide solution was introduced between the gold slide and the window. The following are the corresponding microscope parts: (B) 1064-nm interference filter, (C) camera lens, (D) grating, (E) 10× objective, (F) 1064-nm holographic notch filter, (G) 532-nm holographic notch filter, (H) tube lens, and (I) CCD camera.

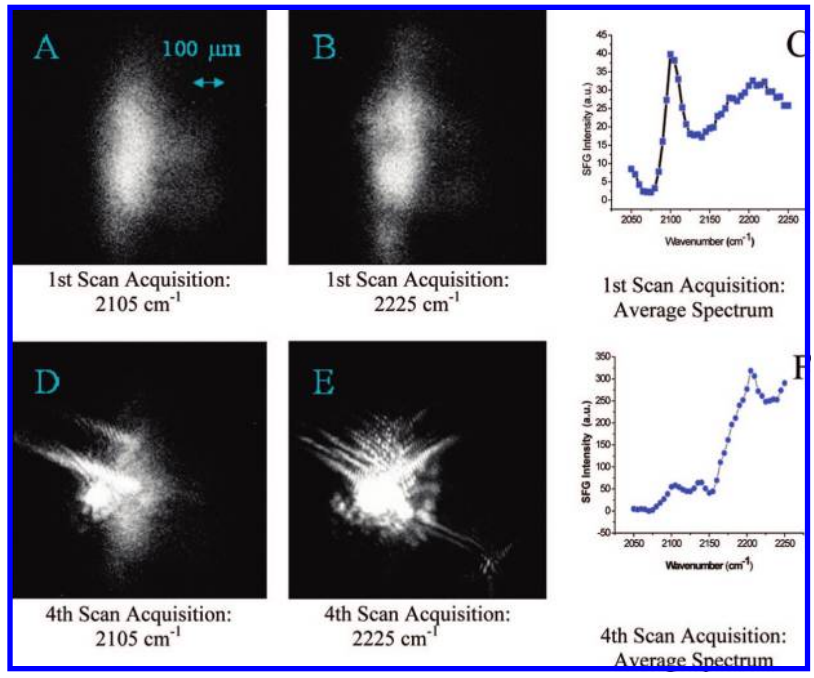

Figure 2. (A, B) SFG images of gold film's initial reaction to 0.5 M CN^- solution acquired at 2105 and 2225 cm^{-1}, respectively. (C) Average spectrum of the first scan acquisition upon exposure of gold film to cyanide solution. (D, E) SFG images acquired approximately after 8 h of exposure to the reactive cyanide solution. (F) Average spectrum of the last scan acquisition (after 8 h).

chromium was evaporated onto the polished side of the wafer to enhance the adhesion of the gold film on the surface. Using the thermal evaporation method, we prepared gold films under vacuum (1×10^{-5} Torr) at a rate of 1 Å/s. The gold film thickness was approximately 1000 Å. After evaporation, the Au-coated silicon wafer was evaluated using ellipsometry for the quality of the film and to obtain the ellipsometric constants of the bare gold.[35]

Cyanide Solution Exposure of Gold Film. The wafer was cut into slides (1 cm × 1 cm) in preparation for the experiment, rinsed with absolute ethanol, and dried with nitrogen gas. Then, the slide was placed inside the SFG cell (Figure 1A). A quantity of 2.4505 g of sodium cyanide salt was dissolved in 100 mL of Milli-Q water (18.2 MΩ cm) to prepare a 0.5 M NaCN solution. Twenty milliliters of this solution was added in the SFG cell containing the Au slide inside. Once the slide was exposed to the cyanide solution, the cell was immediately aligned for the SFG imaging microscopy.

Sum Frequency Generation Experiment

Laser and SFGIM. The SFG process involves the overlap of a 1064-nm beam and a tunable IR beam (2000−4000 cm^{-1}). In the

(35) Colorado, R. J.; Villazana, R. J.; Lee, T. R. *Langmuir* **1998**, *14*, 6337.

Scheme 1. Proposed Steps in the Etching Reaction of Gold in CN^- Solution

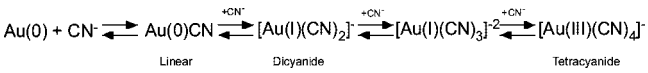

laboratory, a picosecond Nd:YAG Laser (PL2143A/20) was utilized to generate the fundamental wavelength at 1064 nm. The laser has a 20-ps pulse duration and a maximum repetition rate of 20 Hz. The fundamental 1064 beam from the laser pumps the optical parametric generator/amplifier (Laservision) to generate the tunable IR and the 532-nm beam. The microscope was constructed using a reflection configuration. The two beams involved in the SFG process in the microscope setup are the fixed 1064-nm beam and the frequency tunable IR beam (2000−4000 cm^{-1}). Both beams are set to p-polarization, and no output polarizer is used. The 1064 nm beam comes in at an angle of 60°, while the IR beam is at an angle of 70°. When the two beams overlap exactly at the same time and space, the mixing generates the sum frequency generated beam at a specific angle of 62°. The energies of the two beams applied on the surface are the following: (a) 1064-nm beam with an energy density ranging from 50 to 100 mJ/cm^2 and (b) tunable IR beam has an energy around 30−50 mJ/cm^2. Initially, the coherent SFG beam passes through a short pass filter (Figure 1B) to cut off the reflected 1064-nm beam. Then, it passes through a telescope system (Figure 1C) made from Nikon lens to maintain the 1:1 object-to-image size on the grating. A long pass filter was also placed after the telescope to cut off any 532-nm signal generated. The grating (Figure 1D) has the ability to recombine the details of the sample image perpendicularly onto the 10× Mitutoyo objective (Figure 1E). After magnification, a tube lens (Figure 1H) is placed to collimate the beam until it reaches the charged-coupled device (CCD) in Figure 1I (camera; Princeton Instruments) as the detector (with 1024 × 1024 pixel array). Figure 1F,G show the 532- and 1064-nm holographic notch filters, respectively.[36–39]

Image Collection. The images are collected by continuously tuning the IR at 0.02 cm^{-1}/s and acquiring the images for every 5000 shots. Therefore, this process supplies 1 image/5 cm^{-1}. For this time-dependent gold−cyanide reaction experiment, the IR is scanned from 2050−2250 cm^{-1}, collecting 41 images. These images (slices) are stacked using the ImageJ program.[40] Choosing a certain ROI in the stack and by integrating an area gives an intensity value for every 5 cm^{-1}. These SFG intensity values are plotted as a function of the IR wavenumber generating SFG vibrational spectrum.[41–44] Spectra are curve fit to eq 2 for four resonant peaks and a complex nonresonant background. Each image presented is 1 mm^2, and the lateral resolution of this microscope is 10−15 μm. No signal is observe for CN^- at the CaF_2/aqueous interface.

Results

Figure 2A,B shows the SFG images of the gold surface exposed to cyanide solution at 2105 and 2225 cm^{-1}, respectively. These images are slices from the first image stack acquisition from 2000 to 2250 cm^{-1}. These two IR frequencies were chosen because both images represent the linear Au−CN species and the $[Au(CN)_4]^-$ ion which are used as indicators to describe how the gold surface reacts with the cyanide ions (i.e., as the gold progresses from a mono- to tetracoordinated species; Scheme 1).

Figure 2D,E presents images of gold films exposed to cyanide solution after 8 h. These two images are taken from the same location as those in Figure 2A,B at 2105 and 2225 cm^{-1}. On the basis of the observation, these images show more intensity compared to the initial stages of the reaction at the same location, suggesting that more cyanide ions have reacted with the gold atoms generating more corrosion products, $[Au(CN)_4]^-$, and a rougher surface. In addition, the images started to display bright streaks at different positions of the image. This occurrence

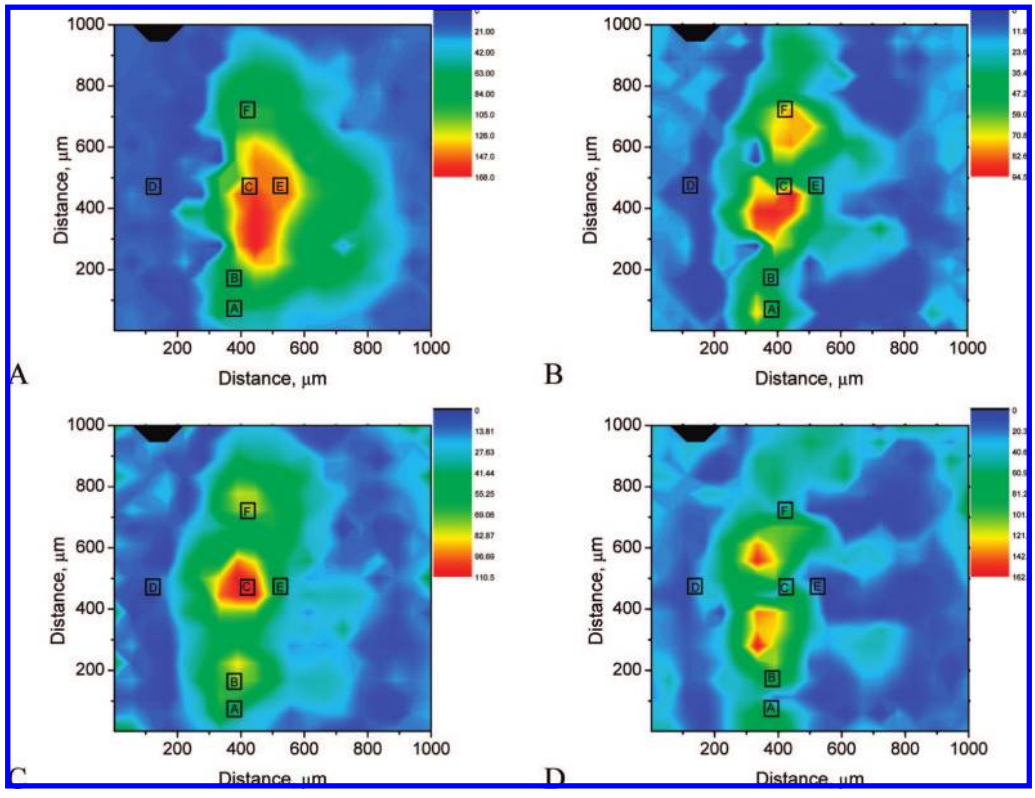

Figure 3. Chemical maps of the C≡N peaks on the gold surface at early stage of the reaction. (A) 2105, (B) 2140, (C) 2170, (D) 2225 cm^{-1}. Labeled areas are ROI A−F.

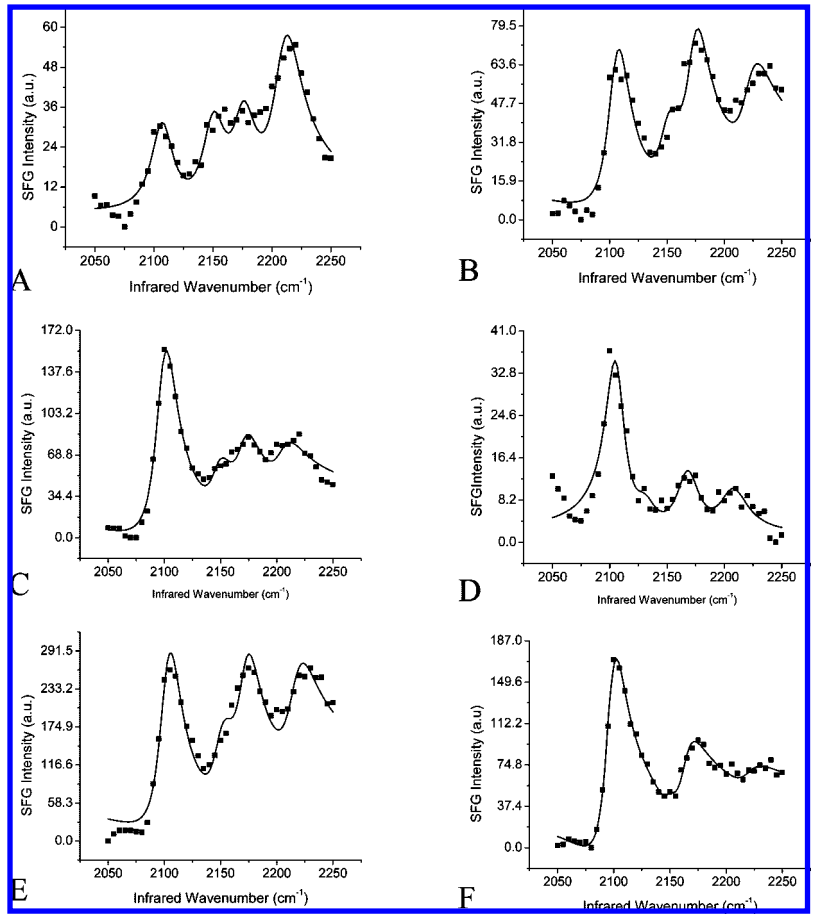

Figure 4. Extracted SFG spectra from selected 50 × 50 μm^2 regions of Figure 3. The line through the data points is a curve fit to eq 2 using four resonant peaks and complex nonresonant background.

is believed to be due to coherent/diffraction effects of the SFG signal. The intensity differences at different parts of the image are related to the dissolution of Au film which forms Au(III)−cyanide precipitates. Once precipitates form, in turn, pit formation occurs, and this creates the rough gold surface. The diffracted beam is observed which results in the coherent effects that are shown in the images.[19]

The spectrum presented in Figure 2C is an average spectrum of the entire probe area. The most dominant peak observed from this spectrum is at 2105 cm^{-1}, which is assigned as the linearly attached CN to one Au atom.[45] The intensity at higher frequencies is due to the combination of three overlapping peaks. The chemical maps (Figure 3) provide a method to resolve these species by their specific locations on the surface.

On the other hand, the spectrum shown in Figure 2F is the average of the surface after 8 h of exposure to CN^- solution. From the plot, four peaks positioned at 2105, 2140, 2170, and 2225 cm^{-1} are observed. The last two peaks are convoluted with each other. The peak at 2170 cm^{-1} is likely due to the Au(III) complex, whereas the most prominent peak is at 2225 cm^{-1}, which is assigned to be either the Au (III) cyanide complex, O−CN^-, or AuCN in solid form.[3,15,17]

Discussion

Chemical Maps. The chemical maps are created from the SFG spectral images. In each experiment, 41 images are acquired, from 2050−2250 cm^{-1} for every 5 cm^{-1}, to create the image stack. An SFG spectrum is extracted from a 50 × 50-μm box that is moved across the image to obtain 400 spectra using the ImageJ program.[40] The spectra are curve fit to extract the peak position, amplitude, and width. The extracted amplitude values are then mapped back onto the surface to provide a spatial location for the different Au−CN species shown in Figure 3.[42]

The chemical maps in Figures 3 and 5 provide a means to visualize the distribution of Au−CN species across the gold surface. Images in Figure 3A−D display the amplitude distribution for the 2105, 2140, 2170, and 2225 cm^{-1} peaks, respectively. The color scale indicates relatively low peak amplitudes in blue and high peak amplitude in red that were determined by spectral curve fitting of the extracted spectra. As seen in the images, the locations with red-yellow have high amplitude and thus are related to the location of higher concentration of corrosion products (Au−CN complexes), while the blue regions are typically dominated by the linear bound CN^- species.

Initial Reaction. To illustrate the variation of Au−CN species across the surface, SFG spectra at six selected regions are

(36) Kuhnke, K.; Hoffmann, D. M. P.; Wu, X. C.; Bittner, A. M.; Kern, K. *Appl. Phys. Lett.* **2003**, *83*, 3830.
(37) Hoffman, D. M. P.; Kuhnke, K.; Kern, K. *Rev. Sci. Instrum.* **2002**, *73*, 3221.
(38) Hoffman, D. M. P. *Nonlinear Spectrosc. Proc. SPIE* **2002**, *4812*, 82.
(39) Chastang, J. C. *Proc. SPIE* **1983**, *399*, 239.
(40) Daniels, M. *Spectrum Extractor for Image J Program*; 1.3.1 ed.; National Institutes of Health: Bethesda, MD, 2004.
(41) Cimatu, K.; Baldelli, S. *J. Phys. Chem. B* **2006**, *110*, 1807.
(42) Cimatu, K.; Baldelli, S. *J. Phys. Chem. C* **2007**, *111*, 11751.
(43) Cimatu, K.; Baldelli, S. *J. Phys. Chem. C* **2007**, *111*, 7137.
(44) Cimatu, K.; Baldelli, S. *J. Am. Chem. Soc.* **2006**, *128*, 16016.
(45) Stuhlmann, C.; Villegas, I.; Weaver, M. J. *Chem. Phys. Lett.* **1994**, *219*, 319.

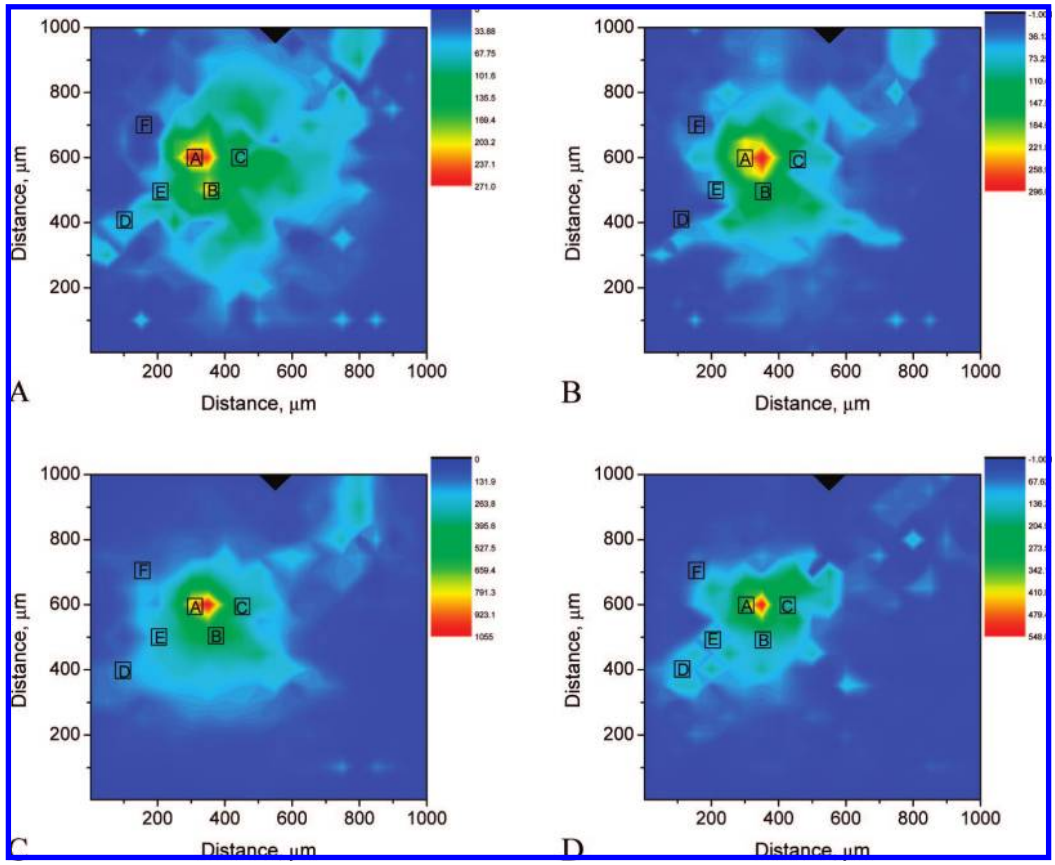

Figure 5. Chemical maps of the C≡N peaks on the gold surface after 8 h of reaction. (A) 2105, (B) 2140, (C) 2170, and (D) 2225 cm^{-1}. Labeled areas are ROI A−F.

presented in Figure 4. The selected regions are 50 × 50 μm^2 and are labeled A−F (ROI A−F). ROI A is located in an area of medium intensity for all four peaks in the spectrum, green zone. The color scale for each peak is only useful for comparisons of the same species and reveals the distribution of that species across the surface and does not necessarily determine the local concentration of one species to another based on this scale. The amplitude in an SFG spectrum is dependent on concentration, orientation, and SFG cross section of each Au−CN species. The spectrum of region A is shown in Figure 4A.

Approximately 100 μm up from region A is region B. The SFG spectrum shown in Figure 4B indicates a change in composition of the surface, as the 2105 cm^{-1} peak has increased in amplitude relative to the other three peaks. Examination of the SFG maps in Figure 3 indicates this; as the red area is approached, the other peaks are at approximately the same amplitude level. Close to the center of the image (ROI C) the SFG spectrum is dominated by the linear bound CN^-; however, there is a substantial amount of the multi-CN-coordinated Au, as indicated by the peaks at 2140, 2170, and 2225 cm^{-1}. This center region is an area of high activity for the linear Au−CN and the $[Au(CN)_2]^-$ species, as seen by the red color in the maps, while the $[Au(CN)_4]^-$ is more concentrated above and below this region (ROI A and B).

Away from the center of the image, the blue color suggests lower corrosion activity. This region, ROI D, is even more clearly dominated by the linear Au−CN, with much smaller contribution from the higher-order Au−CN complexes.

At the boundary between the higher (orange) and lower (blue) corrosion activity is ROI E. There is a mixture of Au−CN species, as shown in Figure 4E. Finally, at the upper location (ROI F) of the image the region is covered predominantly by Au−CN and $[Au(CN)_2]^-$ species (Figure 4F). These maps clearly show a variety of Au−CN complexes on the surface, with spatially distinct locations. The presence of higher-order complexes from linear to the tetracoordinated complex is an indication of the progression in the corrosion reaction. Thus, these maps provide the molecular-level information on the distribution of corrosion products at the solid−liquid interface, based on the vibrational spectrum.

Reaction after Eight Hours. The progress of the corrosion reactions is also followed by the time-dependent images and spectra. Figure 5A−D shows the chemical maps obtained after 8 h of exposure of gold to cyanide solution. Figure 5A represents the chemical map taken at 2105 cm^{-1} which is the linearly bound CN^- ion on Au. There are six regions of interest chosen in the image with 50 × 50 pixel area (ROI A−F). ROI A was selected almost at the point of highest intensity and has different peak intensity distribution from those at earlier times (Figure 4A−D). On the basis of the map and spectrum (Figure 6A), ROI A was close to an area where there is more corrosion products and activity and more di- and tetracoordinated complexes, compared to the monocoordinated cyanide. Region B has the same number of peaks; however, it has different intensity values for each peak compared to that of ROI A and contains the multicoordinated complexes and the linearly bound CN^- to Au. Region B has a transition from red to yellow green (Figure 5A−D); the image is more dominated by the 2170 cm^{-1} species, either $[Au(CN)_2]^-$ or $[Au(CN)_4]^-$. ROI C positioned close to ROI A is almost the same with region B. The region was chosen because it is close to an area with more corrosion

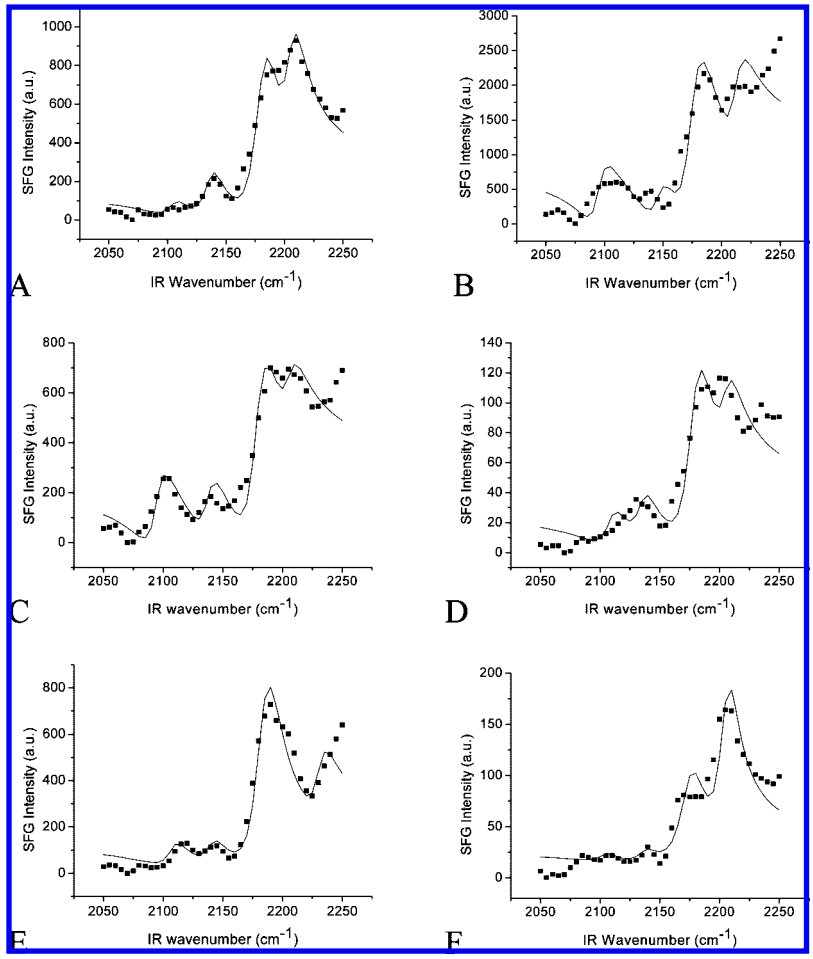

Figure 6. Extracted SFG spectra from selected 50 × 50 μm^2 regions of Figure 5. The line through the data points is a curve fit to eq 2 using four resonant peaks and complex nonresonant background.

products. The di- and tetracoordinated cyanide complexes dominated the area compared to the 2105 cm^{-1} peak. A significant contribution of the 2140 cm^{-1} peak is seen at ROI D, suggesting that the $[Au(CN)_2]^-$ species is significant but still has a contribution from all four complexes.

Region E is positioned close to the border between blue and light blue, as observed. The four peaks are still present with different relative peak amplitudes compared to other regions, and both 2170 and 2225 cm^{-1} have the highest amplitude in the spectrum. Lastly, ROI F is dominated by the 2170 cm^{-1} peak compared to the other three peak positions. The four peaks are still present but with different contributions. The SFG images after eight hours contained the four peaks with peak intensity contributions different from those at the onset of the reaction. As the reaction proceeded, the total SFG intensity across the surface increased, which provided good contrast in the chemical maps (note scale on maps). Further, the progression from mono- to tetracyanide-coordinated species and general increase in corrosion products were observed using the SFG chemical maps.

Selected Regions of Interest. Figures 4 and 6 presents spectra obtained from specific regions as indicated in the chemical maps (Figures 3 and 5). This is to demonstrate that the initial exposure of the gold metal to the cyanide solution shows a set of spectra for specific regions with different number of peaks which pertain to different $C{\equiv}N^-$ on gold.

The simultaneous presence of the different species from the reaction of gold to aqueous cyanide solution suggests that the surface is heterogeneous. Various areas of the gold reacted with cyanide faster than the rest. This is shown by the areas with a pronounced peak at 2225 cm^{-1} ($[Au(CN_4)]^-$), while other locations have the 2105 cm^{-1} peak more prominent, indicating coverage of the linear species (Au−C≡N). This observation is due to many factors such as the local quality of the gold substrate (polycrystalline gold), concentration of the cyanide solution, and exposure time. The observations obtained from the images have led to an interesting conclusion that it is possible to have three or more species present at a certain period of time where the local composition is variable. The presence of the other cyanide complexes might also occur at the surface where they are outside the detection limit of the SFGIM.

Figures 5 (chemical maps) and 6 (spectra obtained in regions A−F) are obtained from a set of data after 8 h of exposure to cyanide solution. At this point, the surface is dominated by Au(III) cyanide complex/AuCN solid at 2225 cm^{-1},[19] though some regions of the images still contain the linearly bound species which has a smaller contribution to the whole image compared to the rest of the peaks positioned at 2140, 2170, and 2225 cm^{-1}. Consequently, the images presented in Figure 2D,E have more contrast (which leads to a better signal-to-noise ratio) compared to the initial set of images, Figure 2A,B. This is due to a lengthened exposure time of the gold metal to the cyanide solution. Then, as a result, the reaction starts to form more gold cyanide complex species/corrosion products compared to the number of linearly attached cyanide species to gold

starts to decrease in number. The formation of the gold cyanide complexes, which are often present only in bulk solution, is observed at the surface in a semisolid form (precipitate). The cyanide species detected by SFG imaging microscopy are the peaks present at 2140 and 2170 cm^{-1} (as the Au(I) and Au(III) cyanide complexes, respectively).[7,12]

After several hours, the intensity in ROI A of Figure 5 increased. This result is suggestive of increased reactivity in this location. Similarly, this region correlated well with the high activity for the $[Au(CN)_4]^-$ chemical map of Figure 3D. At the early stage of the reaction, the tetracyano complex appears concentrated in this area, thus suggesting the reaction has proceeded the furthest at this location.

Then, aside from the spectral response, this surface solid form of the Au(I)/(III) cyanide complexes leads to the coherent interference effect because the gold film starts to form precipitates that cause heterogeneity and roughness across the surface. Roughness on the surface causes the bright diffraction pattern on the images because of the scattering of light when beams strike an uneven surface. These diffraction lines observed in Figure 2D,E do not appear in the chemical maps and the spectra shown on Figure 6A−F from Figure 4 (ROI A−F). The diffraction lines are optical effects that can also be seen by the CCD camera (sensitive to any source of light ranging from 400 to 900 nm), but these effects are not an SFG signal.

Chemical Imaging with SFGIM. The imaging capability of the SFGIM is able to compare the average spectrum (Figure 2A,B and 2E,F) with the localized spectra collected and shown in both Figures 4 and 6. Thus, after comparison, it is suggested that an average spectrum is an approximate representation of the surface. Because of a limited ability to choose any localized region of interest in a sample, an average spectrum of the gold−cyanide reaction does not fully describe or represent the entire result of an experiment in terms of the cyanide species present on the gold surface. In this case, an ability to spatially select the areas of interest and to analyze them individually is an advantage for surface chemistry studies. An addition to this is also the ability to identify the molecules at the surface specifically (vibrational spectroscopy). The microscope was able to distinguish the varying gold cyanide species across the surface of the gold film. The results showed that, at different regions of interest, the spectrum contains one, two, three, or four vibrational peaks. It is possible to obtain the orientation of the cyanide species attached on gold atoms at the interface from fitting results, but in this experiment this analysis was not done. The most important achievement of this experiment was the ability to observe the in situ reaction of gold metal surface during exposure to aqueous cyanide solution as a chemical etchant. This ability to observe the reaction taking place locally is one of the objectives of sum frequency generation imaging microscopy.

Conclusions

SFG imaging was used to demonstrate the spatial and temporal evolution of Au−CN species during the corrosion reaction at the solid−liquid interface. The results showed that the initial species was the chemisorbed linear Au−CN. However, as the reaction progressed, the higher-order $[Au(CN)_2]^-$ and $[Au(CN)_4]^-$ reaction products appeared at specific locations on the surface. Further, SFGIM demonstrated the ability of spectroscopic imaging to develop chemical maps of the surface and the localized nature of this corrosion reaction.

Acknowledgment. We thank the T. R. Lee group for the gold films and support from the ACS-PRF AC (G093213) and NSF (0650779). In addition, we are grateful to Ekspla for funding to develop the SFG microscope and John Glenn Ramon for designing the software analysis.

JA8011676